Published in final edited form as:
Ann Neurol. 2014 April ; 75(4): 508–524. doi:10.1002/ana.24100.

Prenatal cerebral ischemia triggers dysmaturation of caudate projection neurons

Evelyn McClendon, Ph.D.[1], **Kevin Chen, B.S.**[1], **Xi Gong, M.D.**[1], **Elica Sharifnia, B.A.**[1], **Matthew Hagen, B.A.**[1], **Victor Cai**[1], **Daniel C. Shaver, B.A.**[1], **Art Riddle, Ph.D.**[1], **Justin M. Dean, Ph.D.**[6], **Alistair J. Gunn, M.B.Ch.B., Ph.D.**[6], **Claudia Mohr, Ph.D.**[2], **Joshua S. Kaplan, B.A.**[2], **David J. Rossi, Ph.D.**[2], **Christopher D. Kroenke, Ph.D.**[2,3], **A. Roger Hohimer, Ph.D.**[4], and **Stephen A. Back, M.D., Ph.D.**[1,5,7]

[1]Department of Pediatrics, Oregon Health & Science University, Portland, Oregon, USA [2]Department of Behavioral Neuroscience, Oregon Health & Science University, Portland, Oregon, USA [3]Department of Advanced Imaging Research Center, Oregon Health & Science University, Portland, Oregon, USA [4]Department of Obstetrics and Gynecology, Oregon Health & Science University, Portland, Oregon, USA [5]Department of Neurology, Oregon Health & Science University, Portland, Oregon, USA [6]Department of Physiology, University of Auckland, Auckland, New Zealand

Abstract

Objective—Recently we reported that the neocortex displays impaired growth after transient cerebral hypoxia-ischemia (HI) at preterm gestation that is unrelated to neuronal death but is associated with decreased dendritic arbor complexity of cortical projection neurons. We hypothesized that these morphological changes constituted part of a more widespread neuronal dysmaturation response to HI in the caudate nucleus (CN), which contributes to motor and cognitive disability in preterm survivors.

Methods—*Ex vivo* magnetic resonance imaging (MRI), immunohistochemistry and Golgi staining defined CN growth, cell death, proliferation and dendritic maturation in preterm fetal sheep four weeks after HI. Patch-clamping recording was used to analyze glutamatergic synaptic currents in CN neurons.

Results—MRI-defined growth of the CN was reduced after ischemia compared to controls. However, no significant acute or delayed neuronal death was seen in the CN or white matter. Neither was there significant loss of calbindin-positive medium spiny projection neurons (MSNs)

[7]To whom correspondence should be addressed: Stephen A. Back, M.D., Ph.D., Oregon Health and Science University, Department of Pediatrics, Division of Pediatric Neuroscience, 3181 S.W. Sam Jackson Park Rd, Mail Code L481. Portland, Oregon 97239-3098, backs@ohsu.edu, Phone: 503-494-0906.

Author Contributions: SAB, ARH, CDK, DJR and EM were responsible for study design and manuscript preparation. Fetal surgery was performed at OHSU by EM, MH and AHR and by AJG, AR and JMD at the University of Auckland. Morphometric studies and analysis were done at OHSU by EM, KC, ES, VC and DCS and at the University of Auckland by JMD and AR (white matter neuronal death studies). XG was responsible for tissue processing including immunohistochemistry and Golgi staining. Neuroimaging studies were analyzed by KC under the supervision of CDK. Electrophysiology studies were performed and analyzed by DJR, JSK and CM.

Potential Conflicts of Interest
Nothing to report.

or CN interneurons expressing somatostatin, calretinin, parvalbumin, or tyrosine hydroxylase. Morphologically, ischemic MSNs showed a markedly immature dendritic arbor, with fewer dendritic branches, nodes, endings and spines. The magnitude and kinetics of synaptic currents, and the relative contribution of glutamate receptor subtypes in the CN were significantly altered.

Interpretation—The marked MSN dendritic and functional abnormalities after preterm cerebral HI, despite the marked resistance of immature CN neurons to cell death, are consistent with widespread susceptibility of projection neurons to HI-induced dysmaturation. These global disturbances in dendritic maturation and glutamatergic synaptic transmission suggest a new mechanism for long-term motor and behavioral disabilities in preterm survivors via widespread disruption of neuronal connectivity.

In addition to cerebral palsy, preterm survivors are at risk for a wide range of disabilities that include minor motor dysfunction and disturbances in learning, cognition, visual integration, language processing, attention and socialization.[1] Whereas these diverse disabilities were previously attributed principally to cerebral white matter injury (WMI), disrupted gray matter development increasingly appears to contribute to the global developmental disabilities that occur in 25–50% of preterm survivors.[2] Several large human neuroimaging studies have identified significant reductions in the growth of cortical and subcortical gray matter structures that include the basal ganglia, thalamus and hippocampus.[3]

The major cellular mechanisms related to gray matter volume loss in contemporary populations of preterm survivors remain controversial. Several human autopsy studies of cases with significant periventricular leukomalacia (PVL) found widespread loss of neurons in the cortex, subplate and thalamus.[4–6] Neuronal loss was attributed to retrograde neuroaxonal degeneration related to PVL and to direct deletion of neurons, particularly GABAergic interneurons that appear to migrate through human white matter during the period of high risk for WMI.[7, 8] An alternative mechanism is supported by recent human neuroimaging studies that identified aberrant cortical development in preterm survivors with minimal PVL. These studies found that the normal progressive loss of cortical anisotropy was delayed;[9, 10] consistent with our recent preclinical studies that related delayed loss of cortical anisotropy to widespread arrested maturation of the dendritic arbor of cortical projection neurons.[11]

To further define the pathogenesis of gray matter mal-development, we have employed an *in utero* model of preterm ovine global cerebral HI that closely reproduces the spectrum of cerebral injury observed in preterm human infants.[12] The majority of animals acquire moderate diffuse WMI without the pronounced white matter necrosis that now occurs in only a small minority of human preterm survivors.[13] Notably, these animals also display progressive cortical volume loss that occurs without significant neuronal loss.[11] Rather, volume loss arises from reduced complexity of the dendritic arbor of pyramidal neurons, which comprise the major population of cortical projection neurons. Hence, the response of some populations of immature cortical neurons appears to be biased towards dysmaturation rather than cell death, and may be related to the severity of cerebral HI.

Here we tested the hypothesis that the neuronal dysmaturation observed in response to preterm global cerebral HI is not limited to the cerebral cortex, but also more diffusely

disrupts maturation of other populations of projection neurons in subcortical gray matter. We specifically analyzed the caudate nucleus (CN), which displays reduced growth in human preterm survivors[14, 15] and has been associated with multiple neurobehavioral disturbances. These include minor motor impairment,[16] disturbances in IQ,[16] attention,[17] visual-perceptual learning[18] and executive function.[19] In response to HI, we found a significant reduction in caudate volume. Impaired caudate growth was not consistent with a loss of either GABAergic projection neurons or interneurons. Rather, impaired caudate growth was accompanied by diffuse reductions in the maturation of the basal dendritic arbor of medium spiny neurons (MSNs), which comprise the major efferent projections of the CN. Disturbances in connectivity were supported by a significant reduction in the number of dendritic spines of MSNs as well as functional disturbances in glutamatergic synaptic transmission.

Materials and Methods

All 4 week survival studies were performed in a core facility of the Oregon Health & Science University (OHSU) Department of Comparative Medicine and adhered strictly to protocols that were approved by the OHSU Institutional Animal Care and Use Committee (IACUC). Similarly, the 24 hour survival studies were performed in a core facility of the University of Auckland, New Zealand. Animals were housed in these facilities in individual stalls, and maintained in a climate-controlled environment on a 12 hr light/dark cycle where they had access to food and water.

Animal surgery and cerebral hypoperfusion

Details of the general surgical procedures used in this instrumented fetal cerebral hypoperfusion preparation have been described.[12, 20] Given the large size of the fetal ovine brain, a strength of the experimental design was that the animals analyzed here were previously studied and confirmed to also have diffuse cerebral WMI[13] and dysmaturation of cortical neurons.[11] Time-bred preterm fetal sheep (~26 to 28 weeks human gestation-equivalent) were operated between 90–94 days of gestation (term 145 days). On postoperative day 3–4, sustained cerebral hypoperfusion (30–35 minutes duration) was initiated by bilateral carotid artery occlusion and reestablished by deflation of a brachiocephalic occluder.

Physiological monitoring

Prior to the start of the experiment, catheters of the instrumented twin fetus were connected to pressure transducers and a chart recorder (PowerLab 16/30; ADInstruments) to record the pressure in the left fetal carotid artery relative to the amniotic fluid pressure (mean arterial blood pressure). Fetal heart rate was calculated from triplicate measurements of the arterial pressure pulse intervals over a continuous recording of no less than 20 seconds.

Blood analysis

Four blood samples (1 ml each) were taken anaerobically from the left fetal carotid artery during the course of the hypoperfusion study. The first sample was taken prior to the start of the experiment (baseline), the second sample 5 min after the start of the hypoxia, the third

sample 25 minutes after the start of the occlusion, and the last sample 10 min after the occlusion was reversed (recovery). All blood samples were analyzed for arterial pH, Po_2, and Pco_2 corrected to 39°C, hemoglobin content, oxygen saturation (So_2), and hematocrit (ABL725 blood gas analyzer; Radiometer Medical A/S). Fetuses were entered into the study if they demonstrated normal fetal oxygenation post-operatively.

Tissue collection and processing

The pregnant ewes were euthanized with an overdose of the barbiturate, Euthasol, at 24 hours (control: n = 4; HI: n = 4) and four weeks (control: n = 4; HI: n = 4) after the completion of the occlusion protocol. Fetal brains were collected, weighed, and the cerebellum and brainstem was removed by cutting the cerebral peduncles at the pontopeduncular junction. The remaining tele- and diencephalon was cut into five equivalent coronal blocks in proportion to the distance between the frontal and the occipital poles. The coronal blocks were then hemisected, and the left hemisphere blocks were immersed in 4% paraformaldehyde in 0.1 M phosphate buffer (pH 7.4, 4° C) for 3 to 5 days and then stored in a phosphate-buffered saline (PBS) containing 0.05% sodium azide (NaN_3) preservative at 4°C. Tissue blocks from the right hemisphere were immersed in the AB solution from the FD Rapid Golgi Stain Kit (PK 401, FD Neurotechnologies Inc.) for later processing, as described below. All analyses used anatomically matched regions of the rostral portion of the head of the CN, which extended from the frontal pole of the head of the CN caudally to the emergence of the ventral pallidum (corresponding to sections 0441-0639 in the online Michigan State University sheep brain atlas: https://www.msu.edu/~brains/brains/sheep/index.html). The medial edge of the internal capsule was used to delineate the lateral margin of the CN, while the margin abutting the lateral ventricle served to define the medial border. Consequently, all cell counts, neuronal reconstructions, and volumetric measurements defined as CN in this study were confined to this anatomical area. In instances where we examined the caudoputamen complex, the medial edge of the external capsule served to delineate the lateral border.

Ex vivo MRI and volumetric measurements

Paraformaldehyde-fixed coronal blocks from the left hemisphere containing the caudate and caudoputamen (CPu) complex were used to obtain MRI images. The acquisition of MRI slices was the same previously described.[11] Using the ITK-snap program (http://www.itksnap.org), a mask including the voxels defined as belonging either to CN or CPu was manually created over MRI coronal slices to delineate the previously described mediolateral margins throughout the rostrocaudal region of interest. Briefly, this involved loading the DWI as a grayscale image, adding the FA as an overlay, and then expanding the coronal plane on the image (Fig. 1A). The image was then magnified to fit the computer window and the polygon tool (piecewise linear with a segment length setting of 8) was used to draw the boundaries of the CN (Fig. 1B) and CPu (Fig. 1C). The total volume of comparable anatomical regions of interest throughout the CN and CPu was calculated using ITK-snap.

Immunohistochemistry

After MRI, the left hemisphere coronal blocks containing the caudate nucleus were cut in the coronal plane using a vibrating microtome (VT1200S; Leica Microsystems Inc.) into 50 μm thick serial sections and collected into PBS containing 0.05% NaN_3 for immunohistochemical analyses. MSNs were visualized with a rabbit anti-calbindin D-28k (Calb) primary antisera (CB-38a, 1:10000, Swant), a biotin-SP-AffiniPure goat anti-rabbit IgG (H+L) (111-065-045, 1:400, Jackson ImmunoResearch Laboratories Inc.) secondary antibody and fluorescein (DTAF)-streptavidin (016-010-084, 1:400, Jackson ImmunoResearch). To quantify the percentage of MSNs relative to the total CN neuronal population, we double-labeled sections with a mouse anti-NeuN primary antibody, clone A60 (MAB377, 1:1000, Millipore), which was visualized with rhodamine red-X-AffiniPure goat anti-mouse IgG (H+L) (115-295-062, 1:400, Jackson). Tissue sections were counterstained with Hoechst 33342 (Invitrogen/Life Technologies). Apoptotic cells were visualized with a rabbit anti-activated caspase 3 (AC3) antibody (9661B; 1:500; Cell Signaling Technology) and a fluorescein goat anti-rabbit IgG antibody (FI-1000, 1:200, Vectorlabs). Cell proliferation was visualized with a mouse monoclonal anti-Ki67 antibody (NCL-Ki67-MM1, 1: 200, Leica), biotin-SP-AffiniPure goat anti-mouse IgG (115-065-071, 1:400, Jackson) and rhodamine red-X-streptavidin (016-290-084, 1:400, Jackson). Recently generated neurons were visualized with a rabbit anti-doublecortin (DCX) antisera (ab18723, 1:1000, Abcam), biotin-SP-AffiniPure goat anti-rabbit IgG (H+L) (111-065-045, 1:400, Jackson) and fluorescein (DTAF)-streptavidin (016-010-084, 1:400, Jackson). DCX staining was confirmed with a goat anti-DCX antisera (sc-8066; 1:100, Santa Cruz).

Four GABAergic and one cholinergic interneuron populations were analyzed. Parvalbumin-positive (Parv+) interneurons were visualized with a mouse monoclonal anti-parvalbumin antibody (Code No: 235, 1:1000, Swant), a biotin-SP-AffiniPure goat anti-mouse IgG, Fc_γ fragment specific secondary antibody (1:400, Jackson) and fluorescein (DTAF)-streptavidin. Somatostatin-positive (SST+) interneurons were visualized using a rat anti-somatostatin primary antibody (MAB354, 1:100, Millipore), a biotinylated goat anti-rat IgG secondary antibody (1:200, Vectorlabs) and fluorescein (DTAF)-streptavidin. Calretinin-positive (Calr +) interneurons were visualized with a rabbit anti-calretinin primary antibody (Code No: 7699/3H, 1:2000, Swant), a biotin-SP-AffiniPure goat anti-rabbit IgG (H+L) and fluorescein (DTAF)-streptavidin. Tyrosine hydroxylase-positive (TH+) interneurons were visualized with a rabbit anti-tyrosine hydroxylase primary antibody (1:300, Millipore), a biotinylated goat anti-rabbit IgG (1:200, Vectorlabs) and fluorescein streptavidin (1:400, Vectorlabs). Choline acetyltransferase-positive (ChAT+) interneurons were visualized with a mouse monoclonal anti-choline acetyltransferase primary antibody (ab49382, 1:50, Abcam), a biotin-SP-conjugated goat anti-mouse IgG (1:200, Vectorlabs) and fluorescein streptavidin (1:400, Vectorlabs).

Quantification of AC3- and Ki67-positive cells

To quantify the very low number of apoptotic cells and cellular proliferation in both control (n=4) and HI (n=4) animals at 4 weeks post-HI, we counted all labeled AC3- and Ki67-positive cells within the entire CPu with a 20× objective in a minimum of 3 sections sampled at ~150 μm intervals.

At 24 h after HI, we also quantified the number of apoptotic and degenerating cells present within the white matter (n=4 animals/group) labeled by AC3 and Hoechst 33324. White matter boundaries were initially outlined in StereoInvestigator software (MicroBrightField Bioscience, Inc.) with 2.5× objective, and a minimum of 10 sites were randomly selected for counting in each section. All counts were made under a 40× objection in a minimum of 2 adjacent sections per animal taken at the level of the mid-striatum.

Quantification of medium spiny neurons (MSN) and interneurons

In the fetal ovine CN at the gestational age of our study, Calb-labeled MSNs comprise the major population of neurons.[21] Both dorsoventral and rostrocaudal gradients of Calb-positive (Calb+) neurons have been defined in the adult human CN.[22] These gradients require careful attention to anatomic location when sampling. To control for variations in Calb density not related to ischemic changes, we selected sections of the CN across all brains which were at the same coronal location. In each brain, counts of both Calb- and NeuN-positive cells were made from ~15–20 images/section taken with a 40× objective sampled at regular intervals collected in a grid pattern across the mediolateral and dorsoventral extent of a minimum of 3 sections sampled at ~150 μm intervals. Both NeuN and Calb were counted as separate channels to avoid ambiguity in the assignment of double-labeled cells, and the fraction of total NeuN labeled cells that labeled with Calb was used to estimate the percentage of MSNs within the CN. Interneuron populations were stained for Parv, SST, Calr, TH, and ChAT reactivity. Only the SST and ChAT staining yielded sufficient numbers of cells for quantification. The percentage of SST+ and ChAT+ cells was calculated as described above for MSNs.

Golgi-Cox staining

The right hemisphere of 7–10 mm thick coronal blocks of fresh tissue containing the rostral portion of the CN from 4 week recovery animals (~120–126 days of gestation) were processed for the Golgi-Cox staining method using the FD Rapid Golgi Stain Kit (FD Neurotechnologies Inc.), as described.[11] Briefly, this involved immersion of tissue in the kit's AB solution for two weeks before transferring it into solution C until the blocks sank. Each block was then cut in the coronal plane using a vibrating microtome (VT1200S; Leica Microsystems Inc.) into 200 μm thick serial sections. The sections were mounted onto slides, developed for Golgi stain visualization, and dehydrated in a graded alcohol series, before they were cover-slipped.

MSN sampling criteria and neuronal tracing

Golgi-stained tissue sections were used to assess the dendritic morphology of MSNs with Neurolucida software (MicroBrightField Bioscience Inc.). We chose to analyze MSNs, because they have a unique morphology that is readily distinguished by Golgi stain from other neuronal populations in the CN. For each section, the borders of the tissue were outlined under a 5× objective. Next, under a 20× objective, all fields within the CN were viewed with the meander scan function. All cells with the morphological characteristics of a MSN were selected by placing a digital marker when they met the following criteria: (i) a round, ovoid, or pyramidal-shaped soma; (ii) complete filling of the cell body and processes with Golgi-stained material to allow the visualization of the entire arbor of dendrites and

spines; (iii) neuronal soma and processes not obscured by other neurons, glia, or vasculature; and (iv) neurons exhibiting a complete, complex dendritic arbor with many spines and few truncated or cut processes. No attempt was made to anatomically discriminate between the various subtypes of medium spiny neurons. With this initial selection procedure, ~10–50 MSNs were selected per section per case. Due to the difficulty of morphologically discriminating between a developing or potentially injured MSN and other neuronal cell types, we chose to purposely bias against ourselves by reconstructing neurons with the most complex and spiny arbors that met our criteria for MSNs. Using these criteria, ~30% of our pre-selected MSNs were appropriate for dendritic reconstruction. Under a 63× air objective (NA= 0.70; Leica Microsystems Inc.), the outline of the cell soma and the entire dendritic arbor was traced in the x, y, and z coordinate planes. The outline of the soma was traced at its widest point in the 2D plane to provide an estimate of its cross-sectional area. Dendritic processes were not followed into adjacent sections, and the dendritic diameter was not examined. A total of 121 and 124 MSNs, respectively, were reconstructed in the control and ischemic animals.

As an additional control, we quantified the cell soma area size to analyze the homogeneity of our population. We sorted both groups into 50 μm^2 bins to define the distribution of soma sizes throughout the sample population (area range 164.5–972.25 μm^2). Although the area of the control MSNs was significantly larger than the ischemic MSNs (mean ± SEM HI: 362.6 ± 9.159 μm^2, N=121 MSNs; control: 408.8 ± 10.91 μm^2, N=124 MSNs; p = 0.0013), 81% of the neurons in each group did not differ significantly in soma size (mean ± SEM HI: 375.9 ± 7.782 μm^2, N=101 MSNs; control: 391.4 ± 7.318 μm^2, N=99 MSNs; p = 0.1486). Notably, the significance of the indices of dendritic maturation between these two populations did not change whether we controlled for soma size or not. Hence, all findings were reported with respect to the entire populations that we analyzed.

Analysis of dendritic morphology

The complexity of the dendritic arbor in each MSN was analyzed with NeuroExplorer (MicroBrightField Bioscience, Inc.), with respect to total dendritic length, the number of primary dendrites, nodes (i.e., branch points), branches, and terminal endings. These same metrics were also examined for individual branch orders. As a final measure of dendritic complexity, the Sholl analysis used concentric spheres (Sholl rings), centered on the cell at 5 μm intervals, to calculate the number of dendritic intersections per each Sholl ring.

Dendritic spine analysis

With Neurolucida software, the density of the dendritic spines was quantified on the same population of MSNs sampled for dendritic morphology. With a 100× oil objective (NA= 1.30; Leica Microsystems Inc.), spine density was determined by counting all visible spines on all terminal third-order branches of dendrites that were at least 20 μm long. About 20% of MSNs in both groups did not have dendrites that met these criteria because they were either more complex than or not as complex as the rest of the population. Other neuronal exclusion criteria included dendrites that were incompletely filled or that were obscured by other processes. No distinction was made between subtypes of spines. Spine densities were assessed on a total of 99 MSNs in the control group and 108 MSNs in the HI group. Spine

data were calculated on a per-neuron basis by averaging the spine densities from all assessed dendrites for each neuron. Data are presented as the number of spines per micrometer.

Caudate nucleus *in vitro* slice preparation

Methods for preparation of brain slices and subsequent patch-clamp recording were similar to our previous reports in rodents.[23, 24] and modifications for brain tissue from larger mammals.[25, 26] Upon removal of the brain, the frontal pole (anterior to section 0600 in the online Michigan State University sheep brain atlas: https://www.msu.edu/~brains/brains/sheep/index.html) of one hemisphere of the forebrain was rapidly isolated and immersed in an ice-cold slurry (0–2°C) of low-sodium artificial CSF (aCSF) composed of (in mM): 220 sucrose, 3.2 KCl, 1.2 NaH_2PO_4, 6.0 $MgSO_4$, 10 D-glucose, 26 $NaHCO_3$ and 0.2 $CaCl_2$ that was bubbled for 30 min with 95% oxygen/5% carbon dioxide. The striatum (caudate nucleus, internal capsule and putamen) was micro-dissected from the surrounding cortex, and mounted, parallel to the coronal plane, in a slicing chamber filled with ice-cold low sodium aCSF. Coronal slices (350μm) were made with a vibrating tissue slicer (Vibratome). Slices were incubated in warmed (33±1°C) normal aCSF (in mM): 124 NaCl, 26 $NaHCO_3$, 1 NaH_2PO_4, 2.5 KCl, 2.5 $CaCl_2$, 2 $MgCl_2$, 10 D-glucose, and bubbled with 95%O_2/5% CO_2 (pH 7.4) for one hour after sectioning. This solution contained kynurenic acid (1 mM; Ascent Scientific; UK) to block glutamate receptors to reduce potential excitotoxic damage. Kynurenic acid was omitted from the experimental solutions.

Electrophysiology

Slices were placed in a submersion chamber on an upright microscope, and viewed with an Olympus 60X (0.9 numerical aperture) water immersion objective with differential interference contrast and infrared optics. Slices were perfused with warmed (32–34°C) aCSF at a rate of ~6ml/min. Drugs were dissolved in aCSF and applied by bath perfusion. Visually identified medium spiny neurons (soma size = ~10μm) in the CN were voltage-clamped (Vh = −30mV, to relieve voltage-dependent Mg^{2+} block of NMDA receptors) with patch pipettes, constructed from thick-walled borosilicate glass capillaries, and filled with an internal solution containing (in mM): 130 CsGluconate, 4 NaCl, 0.5 CaCl, 10 HEPES, 5 EGTA, 4 MgATP, 0.5 Na_2GTP and 5 QX-314 (lidocaine N-ethyl bromide; Sigma Chemicals). Solutions were pH adjusted to 7.2–7.3 with CsOH. Electrode resistance was 2 to 4 MΩ. Cells were rejected if access resistance was greater than 10 MΩ.

Analysis of glutamatergic excitatory synaptic currents

To pharmacologically isolate excitatory glutamatergic synaptic currents, all recordings were done in the presence of the $GABA_A$ receptor antagonist, GABAzine (10μM; Ascent Scientific; UK). Electrically evoked glutamatergic EPSCs (eEPSCs) were elicited by placing a large patch-electrode (~2MΩ), filled with aCSF into the slice within 100μm of the recorded cell, and applying brief (100ms) constant current electrical pulses of ~100μA. Although slight adjustments of electrode position and/or stimulus strength were made to ensure stable synaptic responses, neither the stimulus strength or distance from the recorded cell differed between control and HI recordings (stimulus strength was 94.5 ± 2.9 and 106.9 ± 8.6 μA for control and HI recordings respectively; electrode distance was 38.4 ± 3.7 and 51.0 ± 5.0 for control and HI recordings respectively; neither significantly different, P >

0.05). All such electrically evoked synaptic currents were abolished by the subsequent application of the AMPA/kainate and NMDA receptor antagonists, NBQX (25μM) and AP5 (50μM) respectively, confirming that all recorded eEPSCs were glutamatergic, i.e. mediated by AMPA/kainate and NMDA subtypes of glutamate receptors. Cells that did not exhibit stable evoked EPSCs with minor variation in electrode position or stimulus strength (n=3 control and 1 HI cells), and cells that responded to glutamate receptor antagonists in a manner that was inconsistent with known pharmacological actions (n = 2 control and 2 HI cells) were excluded from analysis. eEPSCs were acquired at 20 kHz, filtered at 10 kHz, and their magnitude and kinetics were analyzed with pClamp (v.6.3) software (Molecular Devices). All data are expressed as the mean ± the standard error of the mean. For statistical comparisons between cells from control and HI animals, an unpaired Student's t-test or Mann Whitney Rank Sum test was used (depending on whether the data was normally distributed). In all cases, we set the threshold for significance at $p < 0.05$. The glutamate receptor blockers NBQX and AP5 were from Sigma Chemicals (St. Louis, MO).

Statistical analysis

All data analyses were performed with the Prism 4 statistical software (GraphPad Software Inc.). Data are expressed as means ± 1 SEM. Comparisons of group means for cell counts, dendritic morphology parameters, spine densities, and MRI-defined volume data between age-matched control and ischemic animals were performed with unpaired two-tailed t-tests. Sholl (radius × treatment group) and branch order (branch order × treatment group) analyses of dendritic morphology parameters between age-matched control and HI animals were performed by two-way ANOVA followed by Bonferroni post-hoc tests. A value of $P < 0.05$ was considered statistically significant.

Results

MRI-defined volumetric changes in the caudate nucleus (CN)

To define the response of the CN to preterm HI, we first analyzed the growth of the CN and CPu at 4 weeks after the insult by high field ex vivo MRI (Fig. 1A–C). The volume of the head of the CN in the HI group, four weeks post-insult, was smaller than in age-matched control animals (Fig. 1D; mean ± SEM HI: 114.7 ± 13.5 mm^3, N=4; control: 164.1 ± 9.4 mm^3, N=4; $p = 0.024$). A similar near-significant trend was observed in the CPu (Fig. 1E; mean ± SEM HI: 246.1 ± 37.3mm^3, N=4; control: 331.2 ± 26.8 mm^3, N=4; $p = 0.11$).

Reduced growth of the ischemic CN is not associated with neuronal loss

To determine whether the observed volumetric changes were related to neuronal loss, we quantified the density of total NeuN-labeled neurons in the CN by sampling throughout the rostrocaudal and dorsoventral extent of the head of the CN. Sampling confirmed the presence of cellular density gradients in the preterm CN that were previously identified in adult human CN[22] (Supplemental Figure S1). When the same anatomical levels were analyzed, there were no differences in the density of NeuN-labeled neurons (Fig. 2A–B) between the control and HI groups (mean ± SEM HI: 1010 ± 177 NeuN+ cells/mm^2, N=4; control: 1040 ± 47 cells/mm^2, N=3; $p = 0.89$). We next stained for calbindin (Calb) to quantify the density of MSNs, which are GABAergic projection neurons and the major

population of neurons in the CN. We similarly found no differences in Calb+ neurons (Fig. 2C–D) or the ratio of Calb/NeuN (Fig. 2E–F) in control versus HI treated animals (mean ± SEM HI: 493 ± 49 Calb+ cells/mm^2, N=4; control: 511 ± 14 cells/mm^2, N=3; p = 0.78; Calb/NeuN ratio (HI): 51 ± 6.0%, N=4; control: 49 ± 1.3%; N=3; p = 0.80).

We next determined if exposure to preterm HI was associated with a reduction in four populations of GABAergic interneurons in the CN that label with calretinin (Calr, Fig. 3A), parvalbumin (Parv, Fig. 3B), somatostatin (SST, Fig. 3C), or tyrosine hydroxylase (TH). At this time in development, Calr- or Parv-labeled neurons were rarely detected in the CN. Although TH-labeled neurons were visualized in the substantia nigra, no TH-labeled interneurons were present in the CN (Supplemental Fig. S2A and B). SST-labeled neurons comprised less than 1% of the total neuronal population (data not shown) but were sufficiently abundant to quantify. There were no significant differences in density of SST-labeled cells between control and HI groups (Fig. 3D; mean ± SEM HI: 16 ± 4 cells/ mm^2, N=4; control: 10 ± 2 cells/ mm^2, N=4; p = 0.22. There were also no differences in the percentage of total CN neurons (labeled with NeuN) that stained for SST (SST/NeuN ratio: HI = 0.015 ± 0.003%, N=4; control = 0.0099 ± 0.002%; N=4; p = 0.20). Hence, although the CN is largely composed of GABAergic neurons, exposure to HI was not associated with an apparent reduction in either GABAergic projection neurons or interneurons.

In addition to several GABAergic interneuron populations, cholinergic interneurons were visualized that expressed choline acetyltransferase reactivity (ChAT). ChAT-positive neurons (Supplemental Figure S2C and D) were a minor population that comprised ~1% of the total neurons in the CN. There was a significant increase in the density of these interneurons in the HI group (mean ± SEM HI: 14.2 ± 1.9 cells/ mm^2, N=4; control: 7 ± 1.8 cells/ mm^2, N=4; p = 0.03).

Reduced growth of the ischemic CN is not associated with acute or delayed neuronal death

We next determined whether reduced CN growth was related to acute or delayed neuronal death. Since GABAergic neurons appear to migrate through human white matter during the period of high risk for WMI, it has been hypothesized that neurons migrating through the white matter are particularly susceptible to cell death and are reduced in number in the gray matter structures where their migration terminates.[7] Since the CN is highly enriched in GABAergic neurons, we analyzed the response of white matter neurons at 24 h after HI. In control white matter, numerous NeuN-positive neurons were visualized throughout the preterm cerebral white matter at 0.65 gestation when animals were exposed to HI (Fig. 4A). In response to HI, numerous cells were found to acutely degenerate that labeled with activated caspase 3 (Fig. 4B; AC3) or which contained a degenerating nucleus visualized with Hoechst 33324 (Fig. 4C). However, none of the cells expressed NeuN (Fig. 4D). We also found no evidence of recently generated neurons in the white matter of the control or H-I groups, as assessed by doublecortin (DCX) staining (data not shown).

To address the possibility that reduced CN growth was associated with a combination of delayed apoptosis and compensatory cellular proliferation at 4 weeks, we analyzed the CN for the presence of cells labeled for activated caspase-3 (AC3, figure 5A–B) and Ki67

(figure 5C–D), respectively. There were no differences in the very low magnitude of neuronal death observed between the control and HI groups (Fig. 5B; mean ± SEM HI: 70 ± 3 AC3+ cells in the entire CPu, N=4; control: 57 ± 8, N=4; p = 0.20). Likewise, no differences were detected in the amount of cell proliferation between the two groups, as defined by staining for Ki67 (Fig. 5D; mean ± SEM HI: 95 ± 14 Ki67-positive cells, N=4; control: 80 ± 12, N=4; p = 0.45).

We also found no evidence of recently generated neurons in the CN as assessed by doublecortin (DCX) staining at either 24 hours or 4 weeks after HI (Fig. 6A–D). In contrast, DCX+ neurons were abundant in more superficial layers of the neocortex (Fig. 6E–F) at 4 weeks, consistent with prior observations that later born neurons migrate to more superficial layers of the cortical mantle.[27] Collectively, these data support that at 4 weeks after HI, there was no apparent loss of CN neurons from either early or delayed neuronal death that was consistent with the volumetric changes in the CN.

Volumetric loss in the CN is related to disturbances in dendritic arborization

We next analyzed the dendritic arbors of Golgi-impregnated MSNs since they are the major population of projection neurons in the CN. For multiple measures of basal dendritic complexity, the controls (Fig. 7A) were more mature than neurons from the HI group (Fig. 7B). Control MSNs displayed more primary dendrites (Fig. 7C; control: 8.2 ± 0.2, N=121 MSNs; HI: 7.0 ± 0.2, N=124 MSNs; p = 0.0002). Compared to the HI group, control MSNs also displayed a greater number of dendritic nodes (Fig. 7D; control: 18 ± 0.6, N=121; HI: 13 ± 0.5, N=124; p < 0.0001), dendritic branches (Fig. 7E; control: 45 ± 1.3; HI: 34 ± 1.2; p < 0.0001), and dendritic endings (Fig. 7F control: 27 ± 0.7; HI: 21 ± 0.7; p < 0.0001).

To further quantify differences in complexity of the dendritic arbor, a Sholl analysis was also performed. The observed differences in morphology were reflected in fewer intersections in the HI group (Fig. 7G; p < 0.0001, ANOVA) with the most significant differences occurring within 25–75 μm from the center of the cell soma. The observed differences in dendritic nodes, branches and total dendritic length were also noted at the level of individual branch orders (Figs. 7H–J) with the greatest differences seen in earlier branch orders and with the overall numbers of branches declining in the HI group. Collectively, these data are consistent with an overall failure of MSNs to fully mature.

Impaired dendritic arbor maturation is accompanied by reduced dendritic spine density

We next analyzed whether the abnormal maturation of the dendritic arbor of MSNs was accompanied by disturbances in spine density, a measure of neuronal connectivity. Since MSN dendritic arbors were generally complex, we chose to sample spine density on terminal tertiary branches (Fig. 8A–D. Neurons exposed to preterm HI had a significant reduction in spines of ~12% relative to controls (Fig. 8E; mean ± SEM HI: 0.66 ± 0.02 spines/μm, N=108; control: 0.78 ± 0.02, N=99; p<0.001).

Altered dendritic spine architecture is associated with altered glutamatergic synaptic transmission

Glutamatergic synaptic transmission, which occurs at synapses located on dendritic spines, is the primary mechanism mediating fast excitatory signaling in the brain. We therefore analyzed slices from fetal sheep striatum to determine if the HI-induced alterations in dendritic and spine architecture at 4 weeks after HI were associated with altered glutamatergic synaptic transmission. In order to record synaptic currents generated by both the AMPA/kainate and NMDA subtypes of glutamate receptors, caudate nucleus neurons were voltage-clamped at −30mV (to relieve voltage-dependent Mg^{2+} block of NMDA receptor gated channels), and all patch-clamp recordings were done in the continued presence of the broad spectrum $GABA_A$ receptor antagonist, GABAzine (10μM, to pharmacologically isolate glutamatergic synaptic currents). Under these conditions, local electrical stimulation in the CN (within 100 μm of the voltage-clamped cell) reliably evoked an excitatory postsynaptic current (eEPSC) in both control and HI neurons (Fig. 9A). Such eEPSCs were qualitatively similar in control and HI neurons, both consisting of a fast rise to peak, followed by a multi-exponential decay, with distinct fast and slow components typical of glutamatergic synaptic currents (Fig. 9A). However, although the peak amplitude of eEPSCs was similar in control and HI cells, the decay of the eEPSC was significantly faster in HI neurons (Fig. 9B–D). Accordingly, in cell by cell comparisons, for a given peak amplitude, the amplitude of the eEPSC at later time points was significantly smaller in HI neurons compared to control neurons (Fig. 9B, E). Bath application of the AMPA/Kainate receptor antagonist, NBQX (10μM) followed by the additional application of the NMDA receptor antagonist, AP5 (50 μM), confirmed that the fast peak and slow tail of the composite eEPSC were mediated, respectively, by AMPA/kainate and NMDA subtypes of glutamate receptors, as is typical for glutamatergic synaptic currents (Fig. 9F, G). Digital subtraction of the components of the composite eEPSC blocked by NBQX and AP5 revealed the isolated respective components (Fig. 9G). Analysis of such isolated AMPA/kainate and NMDA receptor components of the eEPSCs revealed a variety of significant alterations in eEPSCs in HI neurons compared to eEPSCs in control neurons (Fig. 9G–J). In particular, although the peak amplitude of the AMPA component was not affected, the peak amplitude of the NMDA receptor component was significantly reduced in HI neurons, resulting in a significantly reduced ratio of the amplitudes of the respective components in cell by cell comparisons (Fig. 9G, H). As expected, given the reduced amplitude, the area of the NMDA receptor component was significantly smaller in HI neurons, but surprisingly, so was the area of the AMPA/kainate receptor component (Fig. 9I). The reduced area of the AMPA receptor component, despite no change in amplitude, was due to a significantly faster decay rate of the AMPA receptor component in HI cells (Fig. 9J). The decay rate of the NMDA receptor component was not significantly different between HI and control cells (Fig. 9J). Taken together, the data indicate that HI causes substantial and long-lasting (at least 4 weeks) alterations in the properties of glutamatergic synaptic transmission onto preterm fetal caudate nucleus neurons.

Discussion

The pathogenesis of impaired cerebral growth in preterm survivors appears to be multifactorial and includes the influences of nutritional status,[9] iatrogenic factors (e.g., prenatal steroid exposure)[28, 29] and cumulative neonatal stress.[30] Preterm neonates are also susceptible to cerebral HI due to disturbances in cerebral auto-regulation that particularly occur during critical illness.[31] We provide new evidence that global fetal cerebral HI can also adversely affect the growth of the preterm CN through a mechanism that involves disrupted maturation of the dendritic arbor of MSNs, the major population of CN projection neurons. Widespread disturbances in MSN dendritic arbor complexity were accompanied by a significant reduction in spine density. Further, the duration of glutamatergic synaptic currents, which are generated at MSN spines, was significantly shorter, due to alterations in both the AMPA/kainate and NMDA receptor components of the composite synaptic currents. Thus, HI-induced dysmaturation of MSNs provides a potential new explanation for some of the motor, cognitive and learning disabilities commonly seen in preterm survivors that were previously attributed mostly to WMI.

Prior volumetric MRI studies in human preterm survivors at term found significant reductions in the growth of the basal ganglia.[14, 15] From our results, several potential mechanisms for reduced CN growth appear less likely. A reduction in soma size is an unlikely explanation, since ~80% of CN cells displayed no significant differences in the total area of the soma. Moreover, the cell soma comprised a relatively small fraction of the total volume of MSNs, which were typically highly arborized even in the fetal CN at ~0.8 gestation. It has been hypothesized that GABAergic interneurons may be particularly susceptible to HI, because their migration through cerebral white matter coincides with the peak window for vulnerability to preterm WMI.[7] Given that the CN mostly comprises GABAergic MSNs and interneurons, we similarly hypothesized that an HI-related loss of GABAergic neurons occurs in the CN during their migration through the white matter from the ganglion eminences and other sources in the telencephalon.[32] Although numerous neurons are present in the preterm white matter, we detected no acute neuronal degeneration after HI with two distinct cell death markers. Moreover, we found no significant differences in the chronic density of MSNs or SST-positive interneurons to account for a reduction in CN volume. A direct effect of HI on CN neuron survival also could account for CN volume reduction. However, acute cell loss in the CN involved only ~2% of total CN cells,[33] and we also found no evidence of delayed neuronal death. Hence, our impaired CN growth is not consistent with acute or delayed effects of HI on neuronal survival in gray or white matter. Reduced fetal ovine CN growth is thus most consistent with disturbances in maturation of the MSN dendritic arbor.

Abnormal maturation of MSNs supports a mechanism whereby preterm HI appears to cause widespread disturbances in cerebral growth via dysmaturation of the dendritic arbor of projection neurons in multiple brain regions. Expansion of the preterm human cerebral cortex during the latter half of gestation coincides with a period of robust dendritic arborization and synaptogenesis.[34] In response to HI, the fetal ovine cortex also displayed reduced growth that coincided with disturbances in maturation of the dendritic arbor of pyramidal neurons throughout all cortical layers.[11] Consistent with a global effect of HI on

neuronal maturation, we previously found that during global HI, the preterm fetal cerebrum lacked spatial blood flow gradients. Rather, the magnitude of ischemia was very similar in superficial cortex and deeper cerebral structures including the CN and periventricular white matter.[33, 35]

Disturbances in neuronal connectivity were further supported by similar reductions in dendritic spine density on both MSNs and cortical pyramidal neurons. Both populations of projection neurons showed a similar pattern of dendritic arbor simplification that was significantly disrupted closer to the cell soma, a key site for spatial integration of synaptic inputs.[36] Patch-clamp recording of MSN glutamatergic synaptic currents, which are generated at MSN spines, indicated that synaptic excitation of MSNs was substantially altered. In particular, the decay time of the fast AMPA/Kainate receptor component of eEPSCs and the magnitude of the slow NMDA receptor component were significantly reduced. Both of these alterations contribute to a reduction in total amount of excitatory current and a shortening of its duration. Thus, it is expected that afferent excitation of MSNs will be reduced, and will have a shorter time window for synaptic integration of multiple synaptic inputs. Such alterations in MSN excitation and synaptic integration are likely to perturb CN processing and associated behaviors,[37] thereby contributing to the neurobehavioral phenotype of preterm survivors. Additionally, given the role of Ca^{2+} influx through NMDA receptor channels in mediating neuronal migration,[38–42] synapse formation and pruning,[43–47] and other developmental processes,[48–50] our finding of a significant reduction in the NMDA receptor component of eEPSCs could contribute to a vicious cycle of further dysmaturation. Prior studies support that a functional glutamatergic system is present in the preterm fetal brain. Microdialysis studies detected glutamate release in response to preterm fetal ovine H-I[51, 52] and glutamate receptor blockade rendered partial neuroprotection after severe preterm HI.[53] Disturbances in glutamatergic signaling and excitatory synaptic transmission have been defined in rodents in response to neonatal hypoxia and seizures.[54–57] It will thus be important to determine when such changes in synaptic signaling begin during fetal development, how long they persist and to define the mechanisms that trigger and mediate such changes. Such information could provide potential pharmacological targets for ameliorating HI induced neuronal dysmaturation and associated neurobehavioral complications.

The response of neurons to global HI may be related both to gestational age and the duration of HI. Moderately severe HI in our preterm model at 0.65 gestation (equivalent to a ~26–28 week human fetus)[12] did not trigger significant death of neurons in the CN. By contrast, repeated HI via umbilical cord occlusion in the near term fetal sheep caused extensive neuronal degeneration in the CN.[21] Graded cerebral injury in preterm fetal sheep was related to the duration of global cerebral HI.[33] No significant neuronal degeneration occurred in the gray matter unless the duration of HI was sufficiently prolonged to cause more severe WMI that resembled cystic PVL. Diffuse WMI without pronounced white matter necrosis was generated by a shorter duration of HI. Diffuse WMI was characterized by pre-oligodendrocyte (preOL) death and diffuse gliosis that mostly spared neurons and axons.[33] Similarly, moderate human WMI was characterized by preOL loss, but no significant degeneration of cortical neurons or neuroaxonal elements in white matter.[58] It is notable that isolated diffuse WMI was also not associated with significant neuronal loss in the cortex,

basal ganglia, thalamus or cerebellum.[59] Neuronal loss in multiple cerebral regions has been observed principally in autopsy cases where the more significant necrotic white matter lesions of PVL were observed.[4, 5, 59, 60] Such neuronal loss appears to be related to retrograde axonal degeneration in focal necrotic WMI.[20, 61] Collectively, our findings support that diffuse WMI is associated with neuronal dysmaturation rather than neuronal degeneration in both the cerebral cortex and the CN. Diffuse human WMI is characterized by diffuse gliosis and delayed myelination,[62] that has the potential to also disrupt the functional integrity of the axons of projection neurons. This may provide an additional mechanism of neuronal dysfunction, since oligodendrocytes provide metabolic support for axons.[63]

Further studies are required to determine whether neuronal dysmaturation can also occur without WMI. Reductions in cortical growth in contemporary cohorts of human preterm survivors were not significantly associated with WMI,[9] but with abnormally higher fractional anisotropy (FA) measurements. In our fetal ovine model, we replicated cortical volume loss and abnormal elevations in cortical FA and found that they were related to reduced complexity of the dendritic arbor of pyramidal neurons.[11] Future studies are also needed to evaluate other potential mechanisms of neuronal dysmaturation and disrupted neuronal connectivity that may involve subplate neurons that have been shown to be vulnerable to HI.[64]

HI-induced neuronal dysmaturation provides a new explanation for multiple types of sometimes subtle but frequently significant neurobehavioral disturbances that affect preterm survivors.[1, 27] Altered neurobehavior is already detected by term equivalence during neonatal intensive care.[65] Preterm survivors often display transient or persistent disturbances in motor performance (e.g., minor motor impairment, dyspraxia, and transient dystonia), learning, memory, cognition, attention, visual integration and socialization. The global nature of these disabilities is consistent with more widespread dysfunction of the CNS that may be mediated by the less severe type of projection neuron dysmaturation that we observed in the caudate and cortex. Neuronal degeneration and loss may result in more pronounced disabilities including more severe cerebral palsy and mental retardation. Whether neuronal dysmaturation persists indefinitely is not yet known. Future studies are also needed to determine the effects of HI on interneuron maturation. Since disturbances in neuronal maturation occur at a critical window in the establishment of neuronal connections, even transient neuronal dysmaturation may have persistent global effects on the subsequent development of the CNS of preterm survivors.

Supplementary Material

Refer to Web version on PubMed Central for supplementary material.

Acknowledgments

Supported by the NIH (National Institutes of Neurological Diseases and Stroke: 1R01NS054044, and R37NS045737-06S1/06S2 (SAB); National Institute on Alcohol Abuse and Alcoholism: R01AA012439 (DJR) and T32 AA007468 (JSK)), American Heart Association Grant in Aids (SAB, DJR), the March of Dimes Birth Defects Foundation (SAB), The Health Research Council of New Zealand (AJG), Gravida (the National centre for growth

and development; (AJG)) and the Marsden Fund (JMD). The Neuroscience Imaging Center at OHSU is supported by NINDS grant P30NS061800.

References

1. Allen, M. Outcomes after brain injury in the preterm infant. In: Miller, S.; Shevell, M., editors. Acquired Brain Injury in the Fetus and Newborn. London: Mac Keith Press; 2012. p. 99-120.
2. Volpe JJ. Brain injury in premature infants: a complex amalgam of destructive and developmental disturbances. Lancet Neurol. 2009; 8:110–24. [PubMed: 19081519]
3. Keunen K, Kersbergen KJ, Groenendaal F, Isgum I, de Vries LS, Benders MJ. Brain tissue volumes in preterm infants: prematurity, perinatal risk factors and neurodevelopmental outcome: a systematic review. J Matern Fetal Neonatal Med. 2012; 25 (Suppl 1):89–100. [PubMed: 22348253]
4. Andiman SE, Haynes RL, Trachtenberg FL, et al. The cerebral cortex overlying periventricular leukomalacia: analysis of pyramidal neurons. Brain Pathol. 2010; 20:803–14. [PubMed: 20331617]
5. Kinney H, Haynes R, Xu G, et al. Neuron deficit in the white matter and subplate in periventricular leukomalacia. Ann Neurol. 2012; 71:397–406. [PubMed: 22451205]
6. Ligam P, Haynes RL, Folkerth RD, et al. Thalamic damage in periventricular leukomalacia: novel pathologic observations relevant to cognitive deficits in survivors of prematurity. Pediatr Res. 2009; 65:524–9. [PubMed: 19127204]
7. Xu G, Broadbelt KG, Haynes RL, et al. Late development of the GABAergic system in the human cerebral cortex and white matter. J Neuropathol Exp Neurol. 2011; 70:841–58. [PubMed: 21937910]
8. Letinic K, Zoncu R, Rakic P. Origin of GABAergic neurons in the human neocortex. Nature. 2002; 417:645–9. [PubMed: 12050665]
9. Vinall J, Grunau RE, Brant R, et al. Slower postnatal growth is associated with delayed cerebral cortical maturation in preterm newborns. Sci Transl Med. 2013; 5:168ra8.
10. Ball G, Srinivasan L, Aljabar P, et al. Development of cortical microstructure in the preterm human brain. Proc Natl Acad Sci U S A. 2013; 110:9541–6. [PubMed: 23696665]
11. Dean J, McClendon E, Hansen K, et al. Prenatal cerebral ischemia disrupts MRI-defined cortical microstructure through disturbances in neuronal arborization. Sci Transl Med. 2013; 5:101–11.
12. Back S, Riddle A, Hohimer A. The instrumented fetal sheep as a model of cerebral white matter injury in the preterm infant. Neurotherapeutics. 2012; 9:359–70. [PubMed: 22399133]
13. Riddle A, Dean J, JRB, et al. Histopathological correlates of MRI-defined chronic perinatal white matter injury. Ann Neurol. 2011; 70:493–507. [PubMed: 21796666]
14. Srinivasan L, Dutta R, Counsell S, et al. Quantification of deep gray matter in preterm infants at term-equivalent age using manual volumetry of 3-tesla magnetic resonance images. Pediatrics. 2007; 119:759–65. [PubMed: 17403847]
15. Thompson DK, Warfield SK, Carlin JB, et al. Perinatal risk factors altering regional brain structure in the preterm infant. Brain. 2007; 130:667–77. [PubMed: 17008333]
16. Abernethy LJ, Cooke RW, Foulder-Hughes L. Caudate and hippocampal volumes, intelligence, and motor impairment in 7-year-old children who were born preterm. Pediatr Res. 2004; 55:884–93. [PubMed: 14764914]
17. Nosarti C, Allin MP, Frangou S, Rifkin L, Murray RM. Hyperactivity in adolescents born very preterm is associated with decreased caudate volume. Biol Psychiatry. 2005; 57:661–6. [PubMed: 15780854]
18. Narberhaus A, Lawrence E, Allin MP, et al. Neural substrates of visual paired associates in young adults with a history of very preterm birth: alterations in fronto-parieto-occipital networks and caudate nucleus. Neuroimage. 2009; 47:1884–93. [PubMed: 19376244]
19. Nosarti C, Shergill SS, Allin MP, et al. Neural substrates of letter fluency processing in young adults who were born very preterm: alterations in frontal and striatal regions. Neuroimage. 2009; 47:1904–13. [PubMed: 19376243]
20. Riddle A, Maire J, Gong X, et al. Differential susceptibility to axonopathy in necrotic and non-necrotic perinatal white matter injury. Stroke. 2012; 43:178–84. [PubMed: 22076007]

21. Mallard EC, Waldvogel HJ, Williams CE, Faull RL, Gluckman PD. Repeated asphyxia causes loss of striatal projection neurons in the fetal sheep brain. Neuroscience. 1995; 65:827–36. [PubMed: 7609881]
22. Karachi C, Francois C, Parain K, et al. Three-dimensional cartography of functional territories in the human striatopallidal complex by using calbindin immunoreactivity. J Comp Neurol. 2002; 450:122–34. [PubMed: 12124757]
23. Mohr C, Brady JD, Rossi DJ. Young age and low temperature, but not female gender delay ATP loss and glutamate release, and protect Purkinje cells during simulated ischemia in cerebellar slices. Neuropharmacology. 2010; 58:392–403. [PubMed: 19825379]
24. Rossi DJ, Oshima T, Attwell D. Glutamate release in severe brain ischaemia is mainly by reversed uptake. Nature. 2000; 403:316–21. [PubMed: 10659851]
25. Mohr C, Kolotushkina O, Kaplan JS, et al. Primate cerebellar granule cells exhibit a tonic GABAAR conductance that is not affected by alcohol: a possible cellular substrate of the low level of response phenotype. Front Neural Circuits. 2013; 7:189. [PubMed: 24324408]
26. Welsh JP, Han VZ, Rossi DJ, et al. Bidirectional plasticity in the primate inferior olive induced by chronic ethanol intoxication and sustained abstinence. Proc Natl Acad Sci U S A. 2011; 108:10314–9. [PubMed: 21642533]
27. Volpe, JJ. Neurology of the Newborn. Philadelphia: W.B. Saunders; 2008.
28. Tam EW, Chau V, Ferriero DM, et al. Preterm cerebellar growth impairment after postnatal exposure to glucocorticoids. Sci Transl Med. 2011; 3:105ra.
29. Heine VM, Griveau A, Chapin C, Ballard PL, Chen JK, Rowitch DH. A small-molecule smoothened agonist prevents glucocorticoid-induced neonatal cerebellar injury. Sci Transl Med. 2011; 3:105ra4.
30. Smith GC, Gutovich J, Smyser C, et al. Neonatal intensive care unit stress is associated with brain development in preterm infants. Ann Neurol. 2011; 70:541–9. [PubMed: 21976396]
31. Greisen G. To autoregulate or not to autoregulate – that is no longer the question. Semin Pediatr Neurol. 2009; 16:207–15. [PubMed: 19945655]
32. Hamasaki T, Goto S, Nishikawa S, Ushio Y. Neuronal cell migration for the developmental formation of the mammalian striatum. Brain Res Rev. 2003; 41:1–12. [PubMed: 12505644]
33. Riddle A, Luo N, Manese M, et al. Spatial heterogeneity in oligodendrocyte lineage maturation and not cerebral blood flow predicts fetal ovine periventricular white matter injury. J Neurosci. 2006; 26:3045–55. [PubMed: 16540583]
34. Anderson BJ. Plasticity of gray matter volume: the cellular and synaptic plasticity that underlies volumetric change. Dev Psychobiol. 2011; 53:456–65. [PubMed: 21678393]
35. McClure M, Riddle A, Manese M, et al. Cerebral blood flow heterogeneity in preterm sheep: lack of physiological support for vascular boundary zones in fetal cerebral white matter. J Cereb Blood Flow Metab. 2008; 28:995–1008. [PubMed: 18091757]
36. Magee JC. Dendritic integration of excitatory synaptic input. Nat Rev Neurosci. 2000; 1:181–90. [PubMed: 11257906]
37. Grillner S, Hellgren J, Menard A, Saitoh K, Wikstrom MA. Mechanisms for selection of basic motor programs--roles for the striatum and pallidum. Trends in neurosciences. 2005; 28:364–70. [PubMed: 15935487]
38. Rossi DJ, Slater NT. The developmental onset of NMDA receptor-channel activity during neuronal migration. Neuropharmacology. 1993; 32:1239–48. [PubMed: 7509049]
39. Komuro H, Rakic P. Modulation of neuronal migration by NMDA receptors. Science. 1993; 260:95–7. [PubMed: 8096653]
40. Namba T, Ming GL, Song H, et al. NMDA receptor regulates migration of newly generated neurons in the adult hippocampus via Disrupted-In-Schizophrenia 1 (DISC1). J Neurochem. 2011; 118:34–44. [PubMed: 21517847]
41. Reiprich P, Kilb W, Luhmann HJ. Neonatal NMDA receptor blockade disturbs neuronal migration in rat somatosensory cortex in vivo. Cereb Cortex. 2005; 15:349–58. [PubMed: 15269112]
42. Behar TN, Scott CA, Greene CL, et al. Glutamate acting at NMDA receptors stimulates embryonic cortical neuronal migration. J Neurosci. 1999; 19:4449–61. [PubMed: 10341246]

43. Zhang ZW, Peterson M, Liu H. Essential role of postsynaptic NMDA receptors in developmental refinement of excitatory synapses. Proc Natl Acad Sci U S A. 2013; 110:1095–100. [PubMed: 23277569]
44. Henson MA, Larsen RS, Lawson SN, et al. Genetic deletion of NR3A accelerates glutamatergic synapse maturation. PloS one. 2012; 7:e42327. [PubMed: 22870318]
45. Gambrill AC, Barria A. NMDA receptor subunit composition controls synaptogenesis and synapse stabilization. Proc Natl Acad Sci U S A. 2011; 108:5855–60. [PubMed: 21427228]
46. Saneyoshi T, Wayman G, Fortin D, et al. Activity-dependent synaptogenesis: regulation by a CaM-kinase kinase/CaM-kinase I/betaPIX signaling complex. Neuron. 2008; 57:94–107. [PubMed: 18184567]
47. Luthi A, Schwyzer L, Mateos JM, Gahwiler BH, McKinney RA. NMDA receptor activation limits the number of synaptic connections during hippocampal development. Nat Neurosci. 2001; 4:1102–7. [PubMed: 11687815]
48. Uchino S, Hirasawa T, Tabata H, et al. Inhibition of N-methyl-D-aspartate receptor activity resulted in aberrant neuronal migration caused by delayed morphological development in the mouse neocortex. Neuroscience. 2010; 169:609–18. [PubMed: 20497907]
49. Hirasawa T, Wada H, Kohsaka S, Uchino S. Inhibition of NMDA receptors induces delayed neuronal maturation and sustained proliferation of progenitor cells during neocortical development. Journal of neuroscience research. 2003; 74:676–87. [PubMed: 14635219]
50. Nacher J, Rosell DR, Alonso-Llosa G, McEwen BS. NMDA receptor antagonist treatment induces a long-lasting increase in the number of proliferating cells, PSA-NCAM-immunoreactive granule neurons and radial glia in the adult rat dentate gyrus. Eur J Neurosci. 2001; 13:512–20. [PubMed: 11168558]
51. Fraser M, Bennet L, Van Zijl PL, et al. Extracellular amino acids and lipid peroxidation products in periventricular white matter during and after cerebral ischemia in preterm fetal sheep. J Neurochem. 2008; 105:2214–23. [PubMed: 18315562]
52. Loeliger M, Watson CS, Reynolds JD, et al. Extracellular glutamate levels and neuropathology in cerebral white matter following repeated umbilical cord occlusion in the near term fetal sheep. Neuroscience. 2003; 116:705–14. [PubMed: 12573713]
53. George SA, Barrett RD, Bennet L, Mathai S, Jensen EC, Gunn AJ. Nonadditive neuroprotection with early glutamate receptor blockade and delayed hypothermia after asphyxia in preterm fetal sheep. Stroke. 2012; 43:3114–7. [PubMed: 22923445]
54. Rakhade SN, Fitzgerald EF, Klein PM, et al. Glutamate receptor 1 phosphorylation at serine 831 and 845 modulates seizure susceptibility and hippocampal hyperexcitability after early life seizures. J Neurosci. 2012; 32:17800–12. [PubMed: 23223299]
55. Rakhade SN, Zhou C, Aujla PK, Fishman R, Sucher NJ, Jensen FE. Early alterations of AMPA receptors mediate synaptic potentiation induced by neonatal seizures. J Neurosci. 2008; 28:7979–90. [PubMed: 18685023]
56. Jensen FE, Wang C, Stafstrom CE, Liu Z, Geary C, Stevens MC. Acute and chronic increases in excitability in rat hippocampal slices after perinatal hypoxia In vivo. J Neurophysiol. 1998; 79:73–81. [PubMed: 9425178]
57. Peng BW, Justice JA, He XH, Sanchez RM. Decreased A-currents in hippocampal dentate granule cells after seizure-inducing hypoxia in the immature rat. Epilepsia. 2013; 54:1223–31. [PubMed: 23815572]
58. Back SA, Luo NL, Mallinson RA, et al. Selective vulnerability of preterm white matter to oxidative damage defined by F_2-isoprostanes. Ann Neurol. 2005; 58:108–20. [PubMed: 15984031]
59. Pierson CR, Folkerth RD, Billiards SS, et al. Gray matter injury associated with periventricular leukomalacia in the premature infant. Acta Neuropathol. 2007; 114:619–31. [PubMed: 17912538]
60. Nagasunder AC, Kinney HC, Bluml S, et al. Abnormal microstructure of the atrophic thalamus in preterm survivors with periventricular leukomalacia. AJNR Am J Neuroradiol. 2011; 32:185–91. [PubMed: 20930003]

61. Haynes RL, Billiards SS, Borenstein NS, Volpe JJ, Kinney HC. Diffuse axonal injury in periventricular leukomalacia as determined by apoptotic marker fractin. Pediatr Res. 2008; 63:656–61. [PubMed: 18520330]

62. Buser J, Maire J, Riddle A, et al. Arrested pre-oligodendrocyte maturation contributes to myelination failure in premature infants. Ann Neurol. 2012; 71:93–109. [PubMed: 22275256]

63. Lee Y, Morrison BM, Li Y, et al. Oligodendroglia metabolically support axons and contribute to neurodegeneration. Nature. 2012; 487:443–8. [PubMed: 22801498]

64. McQuillen PS, Sheldon RA, Shatz CJ, Ferriero DM. Selective vulnerability of subplate neurons after early neonatal hypoxia-ischemia. J Neurosci. 2003; 23:3308–15. [PubMed: 12716938]

65. Pineda RG, Tjoeng TH, Vavasseur C, Kidokoro H, Neil JJ, Inder T. Patterns of altered neurobehavior in preterm infants within the neonatal intensive care unit. J Pediatr. 2013; 162:470–6 e1. [PubMed: 23036482]

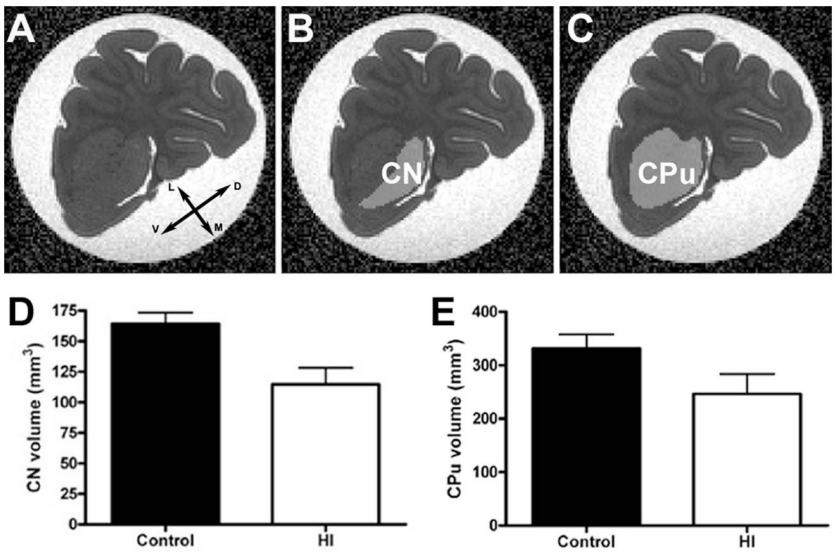

Figure 1.

MRI-defined volumetric changes in the head of the caudate nucleus (CN). (AC) The MRI DWI images were loaded as grayscale images into ITK Snap with FA overlays (A) to serve as a template for the creation of masks (B & C) to measure the volume of the CN (B) and caudoputamen (CPu) complex (C). (D) The CN in the hypoxic/ischemic (HI) group (white bars), four weeks post-insult, is significantly reduced vs. control animals (black bars); $p = 0.024$. (E) A similar near-significant trend was observed in the CPu; $p = 0.11$). Coordinates arrows in A designate dorsal (D), ventral (V), medial (M), and lateral (L).

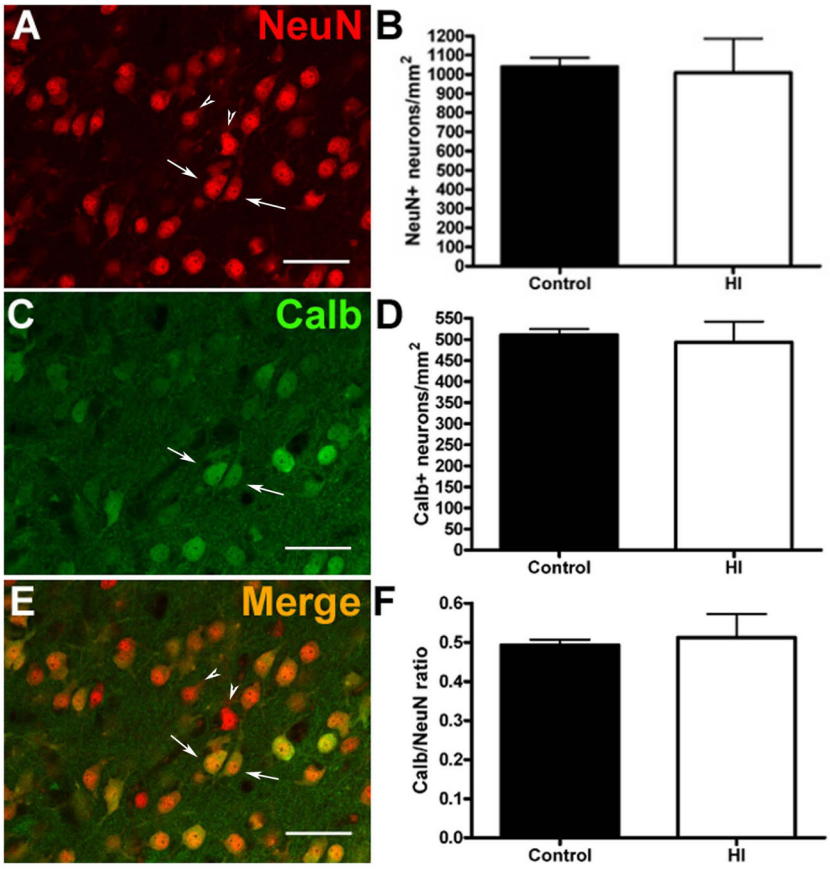

Figure 2.

Volumetric differences in the ischemic CN were not associated with neuronal loss. No significant differences were observed in total neuronal density (A–B), visualized by NeuN immunoreactivity (red channel); p = 0.89 or in the density of MSNs (C–D), visualized by calbindin (Calb) immunoreactivity (green channel); p = 0.78. Arrows indicate examples of cells labeled for NeuN and calbindin and arrowheads indicate cells labeled only for NeuN. (E–F) There were no significant differences in the ratio of calbindin/NeuN in controls vs. the HI group (red-green merge); p = 0.80. Scale bars in A, C, E = 50 μm.

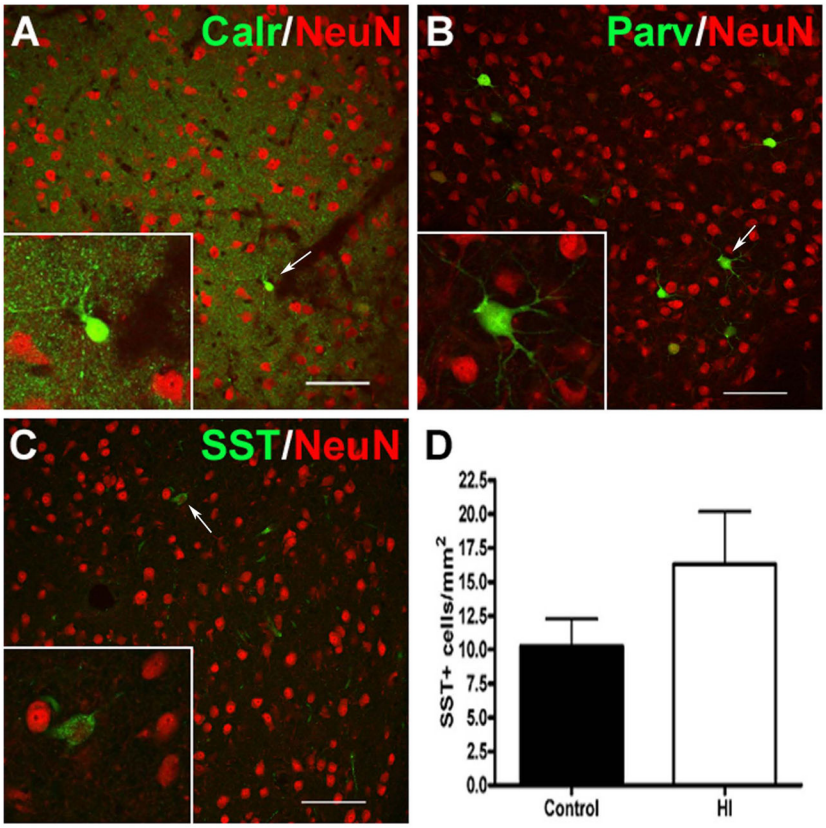

Figure 3.

GABAergic interneuron populations within the CN were sparse as visualized by immunostaining for (A) calretinin (Calr; green), (B) parvalbumin (Parv; green) and (C) somatostatin (SST; green). White arrows indicate the cell shown in each inset. Total neurons were visualized by staining for NeuN (red; A–C). (D) No significant differences in SST density were observed between controls (black bar) and the HI group (white bar); p = 0.22. Images in A–C (20X) represent the highest density region observed for each interneuron marker. Scale bars in A, C, E = 50 μm.

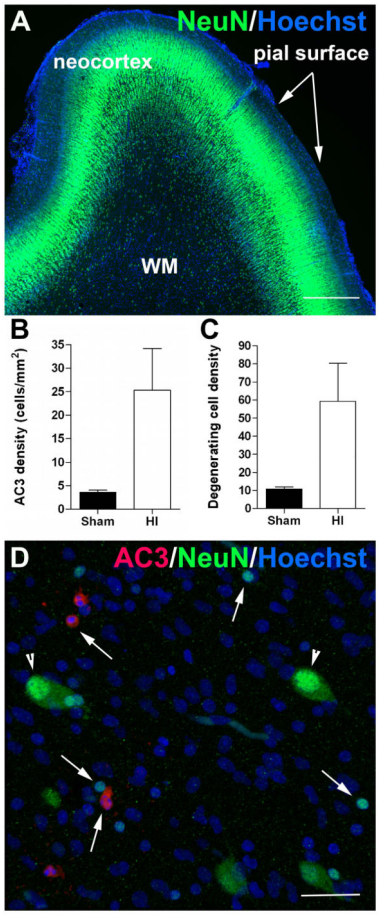

Figure 4.

Neurons in the white matter are resistant to cell death. (A) NeuN-positive neurons (green cells) are abundant throughout the neocortex and white matter (WM) at 0.65 gestational age (GA). (B–C) The density of degenerating cells that labeled for activated caspase-3 (AC3) (B) and Hoechst (C) in the white matter were significantly increased at 24 h after HI at 0.65 GA. (D) Representative photomicrograph of degenerating cells in the white matter at 24h after HI that labeled for AC3 (red cells; arrows) and Hoechst (blue condensed nuclei; arrows). Note the presence of many normal-appearing NeuN-positive neurons (green cells; arrowheads), which showed no evidence of injury. Scale bars A = 500 μm, D = 30 μm. *$p<0.005$.

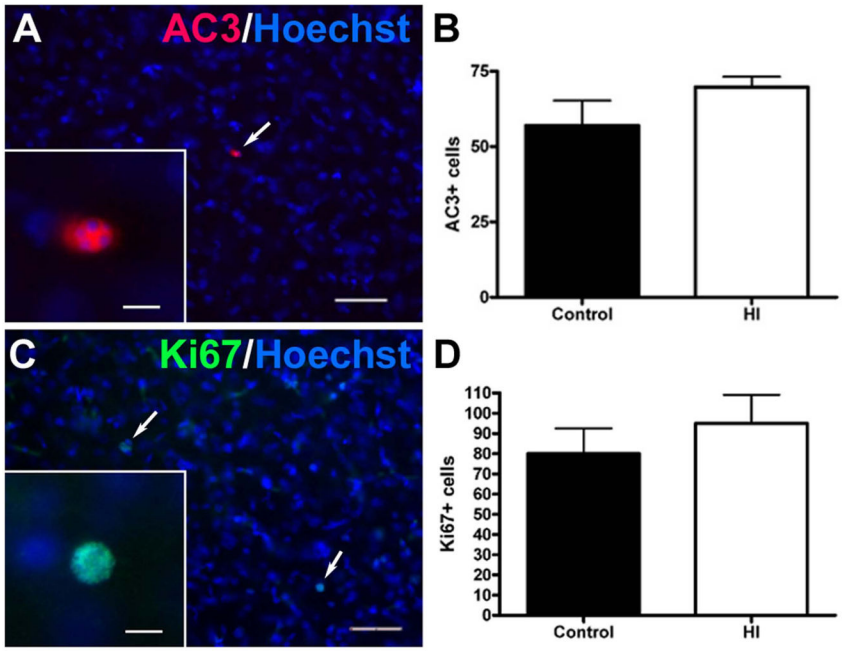

Figure 5.

Reduced growth of the ischemic CN was not associated with enhanced delayed cell death or proliferation at 4 weeks after HI. (A) Typical low density of apoptotic cells (white arrow; inset shows higher power detail), double-labeled with Hoechst (blue) and anti-caspase 3 (AC3; red) antibody. (B) There were no significant differences in the magnitude of apoptosis between the control and HI groups defined by quantification of AC3 labeling in the entire CPu; $p = 0.20$. (C) Typical low density of proliferating cells (white arrows; higher power detail in the inset), double-labeled with Hoechst (blue) and anti-Ki67 antibody (see inset). (D) No differences in cell proliferation were detected between the two groups, as defined by quantification of Ki67 in the entire CPu; $p = 0.45$. Scale bars in A and C = 100 μm; insets = 15 μm.

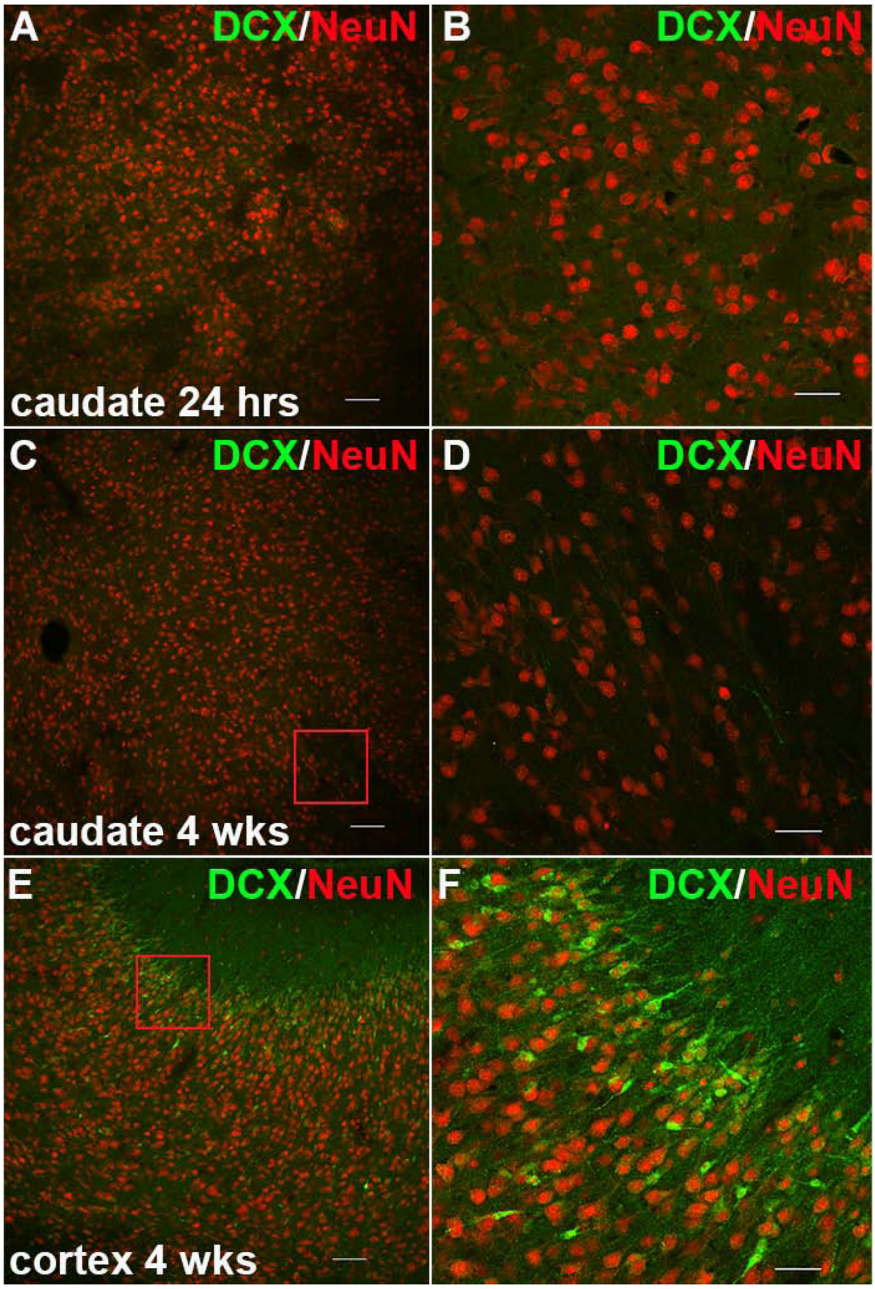

Figure 6.

Recently generated neurons were not visualized in the CN during the acute or chronic phases after HI. (A) Doublecortin (DCX, green) and NeuN (red) staining in the CN 24 hours after HI. (B) A higher magnification image of panel A, which shows that no DCX-positive cells are present. (C) Staining for DCX (green) and NeuN (red) in the CN 4 weeks after HI. (D) A higher magnification image of the red box in panel C, which shows that no DCX-positive cells are present. (E) DCX (green) and NeuN (red) staining in the cerebral cortex. DCX-positive cells were abundant in the superficial layers of the cortical mantle. Panel F is a higher magnification image of the red box in panel E. Scale bars in A, C, and E = 100 μm; scale bars in B, D and F = 50 μm.

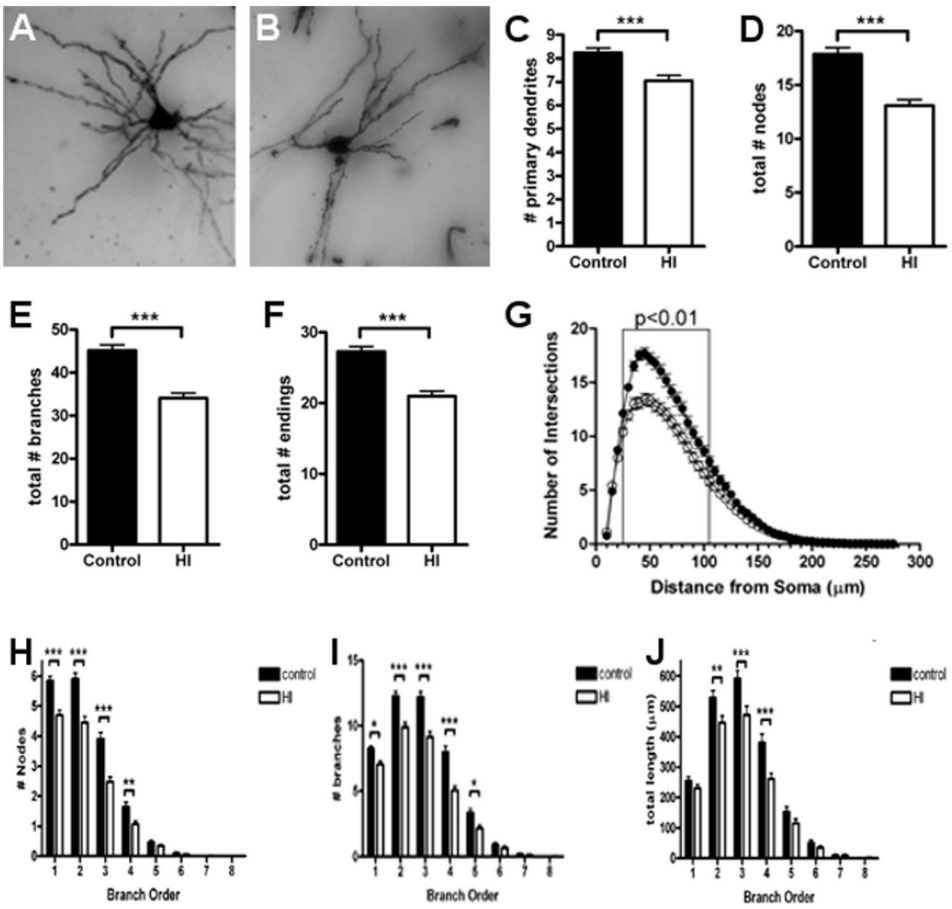

Figure 7.

Abnormal development of the dendritic arbor was seen in MSNs in the CN at 4 weeks after HI. (A) An example of Golgi-stained MSNs is shown for the control (A) and HI groups (B). (C to F) Total number of primary dendritic branches (C), total number of nodes (D), total number of branches (E), and total dendritic endings (F) in the control (black bars) and HI (white bars) groups. (G) Sholl analysis of the number of basal dendritic intersections in control (closed circles) and HI (open circles) groups. (H to J) Branch order analysis of the total number of dendritic nodes (H), total number of dendritic branches (I), total dendritic length (J) in control (black bars) and HI (white bars) groups. n = 121 control and n= 124 HI group cells. Data are means ± SEM. *P < 0.05, **P < 0.01, ***P < 0.001.

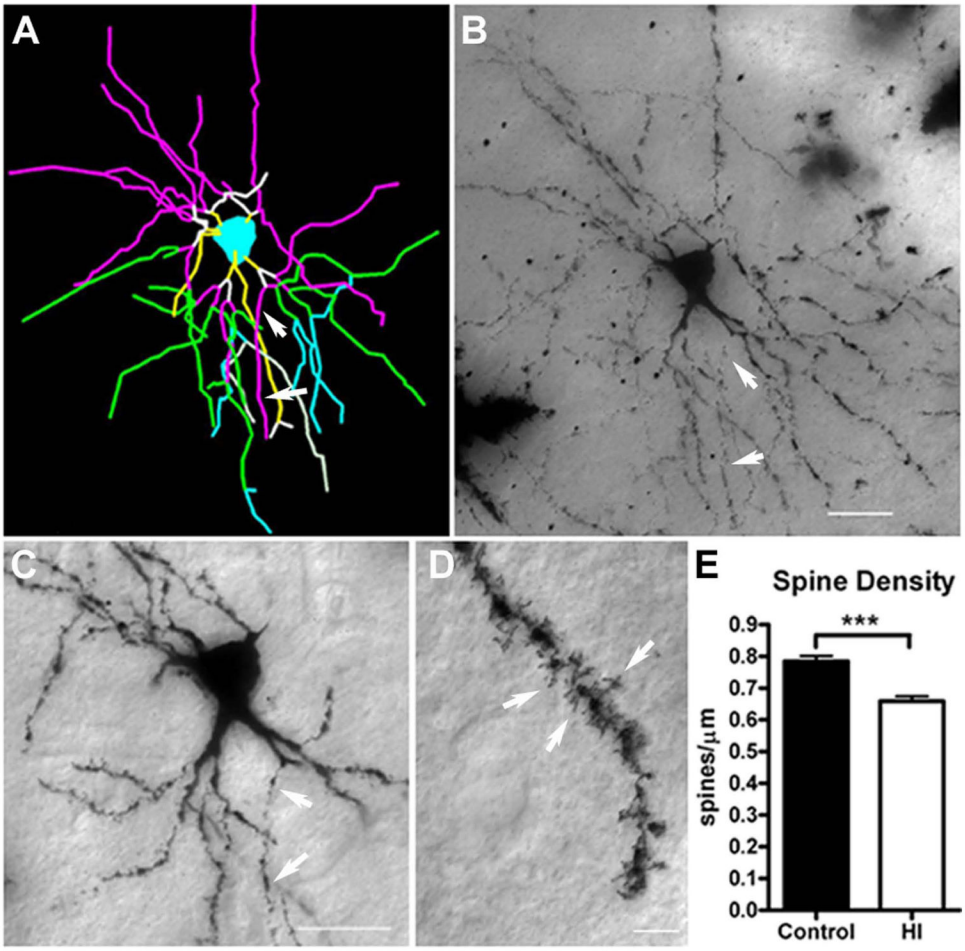

Figure 8.

Impaired dendritic arbor maturation is accompanied by reduced dendritic spine density. For the same population of medium spiny neurons (MSNs) that were sampled for dendritic morphology, spine density was quantified on third-order terminal dendritic branches, which were commonly identified for both groups of neurons. (A–C) Example of third-order terminal branches (white arrows) that were present on the Neurolucida tracing (panel A; purple lines) and the corresponding Golgi-impregnated neuron (B and C). In (A), the yellow, white, purple, green, and blue lines represent first, second, third, fourth, and fifth order branches, respectively. (D) Dendritic spines (white arrows) visualized on a Golgi-impregnated MSN. (E) Spine density in control and HI groups at 4 weeks of recovery. Preterm neurons in the HI group (white bars) had a significant reduction in spines of ~12% vs. controls (black bars); N=108, control and N=99, HI group; $p<0.001$). Scale bars in B, C = 25 µm and in D = 5 µm.

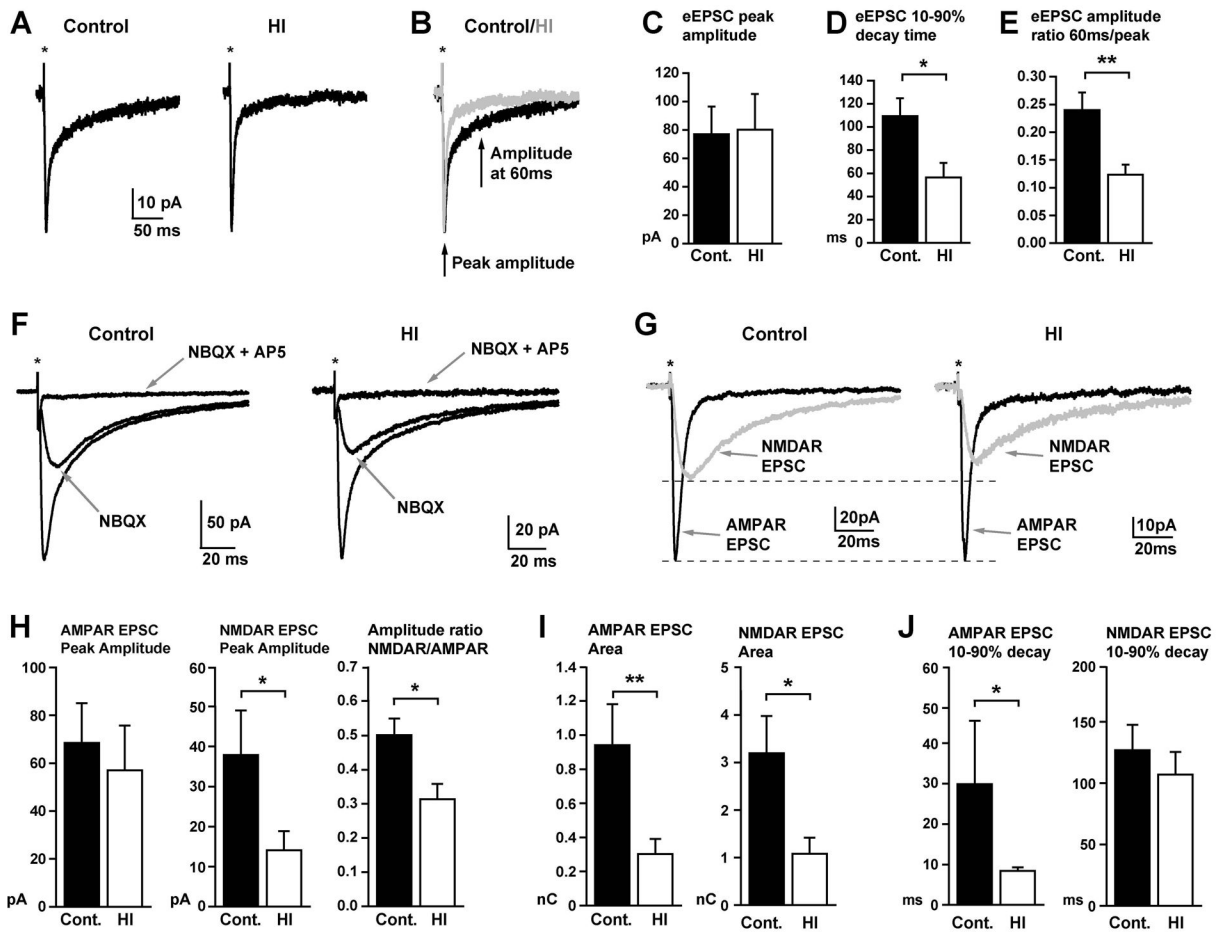

Figure 9.

HI reduces the magnitude, time course and relative receptor makeup of glutamatergic excitatory synaptic currents in caudate nucleus neurons. (A) Representative electrically evoked excitatory postsynaptic currents (eEPSCs) in voltage-clamped (Vh = −30mV) caudate nuclear neurons from control (left) and HI animals (right). Note, to isolate excitatory currents, all recordings were made in the continued presence of the $GABA_A$ receptor antagonist, GABAzine (10μM). (B) Traces from (A) are overlaid in (B) to illustrate faster decay time of eEPSCs in HI cells (gray trace) relative to similar amplitude eEPSCs in control cells (black trace). (C–E) Plots of the mean peak amplitude (C), 10–90% decay time (D), and ratio of amplitudes at late (60ms) and early (peak) time points (E) of eEPSCs in control (black) and HI (white) cells. The peak amplitude of eEPSCs was not significantly different (p=0.84), but the 10–90% decay time was significantly reduced in HI cells (p=0.03), resulting in a significantly reduced amplitude ratio when comparing the amplitude at 60ms and at the peak (p=0.004, n = 9 control and 12 HI cells from 3 animals each). (F) Traces show representative eEPSCs in control (left) and HI (right) neurons, and response to bath application of the AMPA/Kainate receptor antagonist, NBQX (25μM) alone, and then combined with the NMDA receptor antagonist, AP5 (50μM), both indicated by gray arrows. (G) Digital subtraction of traces from (F) reveal the AMPA receptor (black) and NMDA receptor (gray) components of the eEPSC in control (left) and HI (right) neurons. Dashed lines illustrate that when the eEPSCs are scaled to the peak of the AMPA receptor component, the amplitude of the corresponding NMDA receptor component is smaller in HI neurons. (H) Plots of the peak amplitude of the AMPA (left) and NMDA (middle) receptor components, and the corresponding amplitude ratio (right, calculated for the two components in each individual cell) of the eEPSC in control (black) and HI (white) neurons. There were no differences in the amplitude of the AMPA receptor component (p=0.34), but a significantly reduced NMDA receptor component (p=0.04), and correspondingly, the ratio of the NMDA to

AMPA component amplitudes (p=0.02) in HI neurons. (I) Plots showing that the area of both the AMPA and the NMDA receptor components of the eEPSC are significantly reduced in HI neurons (p=0.008 and 0.01, respectively). (J) Plots showing that the 10–90% decay time of the AMPA receptor component is significantly faster in HI neurons (p=0.03), but the decay time of the NMDA receptor component is not significantly different between control and HI cells (p= 0.48). All plots in H to I are from analysis of pharmacologically isolated AMPA and NMDA receptor components of the eEPSC (as shown in F&G) from 8 control and 12 HI cells from 3 animals each. Statistical comparisons were made with a Student's t-test (E, H middle and right plots, I, J right plot) or a Mann Whitney Rank Sum test (C, D, H left plot, J left plot), depending on whether the values were normally distributed.